PROCESSING AND APPLICATION OF MXENE (Ti_3C_2) FOR PLANT NUTRITIONAL STRESS SENSING

A Thesis
Submitted to the Graduate Faculty
of the
North Dakota State University
of Agriculture and Applied Science

By

Sampada Koirala

In Partial Fulfillment of the Requirements
for the Degree of
MASTER OF SCIENCE

Major Program:
Biomedical Engineering

June 2023

Fargo, North Dakota

North Dakota State University
Graduate School

Title

PROCESSING AND APPLICATION OF MXENE (Ti_3C_2) FOR PLANT NUTRITIONAL STRESS SENSING

By

Sampada Koirala

The Supervisory Committee certifies that this ***disquisition*** complies with North Dakota State University's regulations and meets the accepted standards for the degree of

MASTER OF SCIENCE

SUPERVISORY COMMITTEE:

Dr. Danling Wang
Chair

Dr. Qifeng Zhang (co-advisor)

Dr. Ying Huang

Dr. Ewumbua Monono

Dr. Ali Alshami

Approved:

7/5/2023
Date

Dr. Annie Tangpong
Department Chair

ABSTRACT

Environmental stresses cause nutritional stresses which in turn lower crop yields, so understanding this complex relationship can improve crop growth and enable new precision farming methods. The aim of this study is to develop a new nanomaterial MXene-based sensing technology for the detection of the soybean plant nutritional stress released by the plant leaves in order to help plants early diagnosis and disease prevention. When terpenes were applied to MXene material using MILD method, the sensor had a significant response towards alpha-pinene and alpha-humulene with a minimal response showed for linalool terpene. Conversely, terpenes applied to MXene prepared using hydrothermal method showed a significant sensitivity response for only alpha-humulene. Using this low-cost sensing device has opened a new way to detect plant nutritional stress and offer precise measurement for plants growth and health.

ACKNOWLEDGMENTS

I would like to thank my advisor Dr. Danling Wang and Dr. Anamika Prasad from Florida International University who helped me make this research work to be successful. Their guidance and advice helped in all the stages of writing this project. I would also like to thank my co-advisor Dr. Qifeng Zhang for giving me the opportunity to work in his lab, helping me guide ways to become a successful research student and my other committee members for their feedback and helping me defend my thesis successfully.

I would also like to give special thanks to my parents Mr. Sunil Kumar Koirala and Mrs. Shobha Koirala and my brother Dr. Bibhab Koirala for their enormous support, patience, and encouragement. Last but not the least, I would like to thank all of my research group members Dr. Michael Johnson, Aaron Kishlock, and Mahek Sadiq for their support and encouragement during my research study.

DEDICATION

This paper is dedicated to my family as they motivated me to pursue a master's in biomedical engineering program. This would not have been possible without them.

TABLE OF CONTENTS

LIST OF TABLES

LIST OF FIGURES

LIST OF ABBREVIATIONS

MILD .....Minimally Intensive Layer Delamination

FESEM.....Field Emission Scanning Electron Microscopy

XRD .....X-Ray Diffraction

ATR-FTIR.....Attenuated Total Reflection-Fourier Transformed Infrared Spectroscopy

AFM.....Atomic Force Microscopy

1. INTRODUCTION

The ongoing increase in world's population, are greatly affecting the section of agriculture and food supply leading to the shortage of food, pollution challenges due to the use of pesticides, contamination of water and soil, and excessive irrigation demands of agriculture (1-3). Plant diseases are another great concern in the agricultural field as they affect the crops production and quality (4). These factors together have grave consequences in people's lives from long-term sustainability to agriculture-dependent economies worldwide. To address these concerns, it is necessary to develop precision agriculture tools (sensors) and techniques to measure and monitor plants under the influence of the environment and other stresses. Tools that can help to better understand how to maintain plant health as a function of resource utilization are very important in improving efficiencies in crop production. Developing and testing these sensors needs the entire bioengineering and biomedical community to play a critical role.

Nitrogen is a critical element to support plant growth while simultaneously also responsible for soil and water pollution due to excessive use via fertilization (5). An earlier study demonstrated chemical signatures associated with nitrogen usage using RS-based techniques on a longitudinal time-point study of soybean under healthy and nutrition-stressed conditions (4). Among the chemical signatures most affected by reduced nitrogen included a lowering of glutamic acid resulting in lower protein production and a reduction of tetraterpenes and lutein resulting in a lower defense signaling mechanism in the stressed plant. Hence reduction or absence of glutamic acid, tetraterpenes, and lutein all can indicate nutritional stress in plants, and regular sensing of these chemicals can be used in calibrating nitrogen-based fertilizer dispersion on the field. Here, we focus on the defense signaling molecules tetraterpenes for the sensor

development due to their greater sensitivity to nutritional stressors as identified in the earlier work (1).

Currently, there are several techniques which have been used to monitor plant health such as infrared sensors, imaging and image processing, Raman spectroscopy, and hyperspectral imaging, all have been reported to provide information regarding plant growth level and stress (1-3, 6). However, while each of these techniques is important, they are typically time-intensive and expensive either due to equipment cost or the human skills required. Hence, these hindrances prevent its wide use as a convenient tool for regular day-to-day monitoring from small to large farms. Hence, there is a need for a sensitive, but efficient and cost-effective techniques and sensors for in-field deployment.

MXene, a new class of promising material can fulfill this important need for biosensing from precision agriculture to healthcare (6, 7). MXene nanomaterial sensors can offer great advantages which are cost-effective, easy to use, convenient with time, and can provide real-time monitoring for plant growth and health (8). MXene has two-dimensional (2D) architecture like graphene and is a transition metal carbide with a general formula of $M_{n+1}X_nT_x$ ($n = 1-3$) where M is an early transition metal, X is carbon or nitrogen, T signifies a processing-based surface termination groups (-O, -OH, and -F), and x is the number of terminating groups. Compared to other 2D nanostructured materials, such as graphene, metal oxides, and boron nitride (BN), MXenes have similar morphology and electrical characteristics but much broader application due to elemental level permutations possible. They have properties including great biocompatibility, high interlayer spacing and conductivity, and are environmentally friendly which makes this nanomaterial very unique. Over twenty combinations of MXenes have been synthesized with over seventy different compositions being theoretically predicted for different combinations of

M and X (9). This opens new opportunities for the use of 2D MXenes in applications like gas sensing (10, 11), biosensing (9, 12, 13), energy storage devices (5, 14-16), wearable electronics (1, 12), and other high-performance energy applications (17). However, so far, the applicability of this versatile material has not been demonstrated in plant-sensing, specifically for sensing plant nutritional stresses for real-time monitoring of plants growth and health.

MXene nanomaterials were synthesized by exfoliating the MAX-phases where M is a d block transition metal (Ti, Sc, Cr, etc.), A is a III A or IV A group elements, and X is either carbon or nitrogen atoms. The effect of MILD (minimally intensive delamination layer) (18-19) and hydrothermal etching processes (20) on the structure and properties of MXenes were measured (21).

To further explore the synthesis conditions of $Ti_3C_2T_x$, our group synthesized $Ti_3C_2T_x$ at high temperatures and characterized its structure, molecular and surface chemistry, and conductivity as a function of processing conditions. The structure was studied using field-emission Scanning Electron Microscopy (FE-SEM) (22), X-Ray Diffraction (XRD) (23), Attenuated Total Reflection Fourier-Transformed Infrared spectroscopy (ATR-FTIR) (24), and atomic force microscopy (AFM) (25). The as-synthesized MXene was then used in a chemiresistive sensor for VOC detection by measuring changes of its conductivity caused by the presence of relevant plant VOCs associated with the plant nutritional status. Finally, we discuss the relevance and future directions of this study in the context of precision agriculture applications.

Therefore, the main objective of this study was to process $Ti_3C_2T_x$ for the detection of volatile organic compounds (VOCs) released by soybean plants under nutritional stress. The

work builds on soybean plant experiments which identified the chemical signature of nutritionally-stress soybean plant (4).

2. LITERATURE REVIEW

2.1. Soybean Plants

Soybean plants also referred to as Glycine max are polyploidy plants and are among the most important food crops in the world. According to United States Department of Agriculture (USDA), soybeans comprise 90 percent of the U.S. oilseed production such as peanuts, sunflower seed, canola, and flax (26). The market outlook for soybean crops is that the soybean ending stocks in 2023-2024 year in the U.S. has been raised by 15 million bushels to 350 million bushels. In 2022-2023, soybean export forecast has been reduced from 2.015 billion bushels to 2.0 billion bushels due to strong competition from foreign markets. With higher supply and lower domestic demand, soybean meal exports for the 2022-2023 marketing year (MY) have increased by 0.2 million short tons to 14.0 million short tons (27).

2.2. Soybean Terpenes

Soybean plants produce several types of terpenes such as linalool, α-pinene, and α–humulene (28). These terpenes, also known as tetraterpenes, are VOCs released by the soybean plants due to environmental stresses. This stress is released due to the change in various environmental conditions such as high temperature, humidity, soil and water contamination, wind, metal toxicity, ultraviolet radiation, and so on and this cause the levels of the linalool, α-pinene, and α–humulene to be very high (29).

Environmental stresses cause nutritional stresses which in turn lower the crop production, so understanding this complex relationship can improve the overall crop growth and enabling new precision farming methods. Several terpenes have their roles in soybean plant defense against the abiotic and biotic stresses. One of the roles of these terpenes is that it helps in the plant survival and has a defense response mechanism that can help cope with stressors (30).

Some of the tetraterpenes released by soybean plant under environmental stresses are as follows: Linalool is an acyclic monoterpene, meaning it is a type of organic compound consisting of ten carbon atoms arranged in a straight chain. It exists in nature as two enantiomers, which are mirror-image isomers of each other. The two enantiomers of linalool are (R)-(–)-linalool and (S)-(+)-linalool (31). Linalool serves as a biosynthetic precursor to various other alcohols and aldehydes, and plants that express the linalool synthase enzyme that produces different derivatives of linalool, such as linalyl acetate (also known as bergamol) and linalool oxide (32, 33). α-pinene is a major component of the volatile organic compounds released by various plant species worldwide (34). These species include those found in tropical regions, Mediterranean regions (35), and northern coniferous forests (36). Some examples of plants that emit high levels of α-pinene are Eucalyptus, Pine, and Oak, but there are numerous other species, including Salvia, that also emit monoterpenes (37). α-Pinene has been found to have several effects on plants and their physiological processes. For instance, it has been observed to inhibit seed germination and primary root growth in maize. Additionally, it acts as an uncoupler of oxidative phosphorylation and inhibits the electron transport chain, disrupting energy metabolism. In maize roots, exposure to α-pinene has been shown to increase malondialdehyde levels, indicating oxidative stress in the target tissue (38). α-humulene is a sesquiterpene found in various plants, including soybeans. It has a woody and earthy aroma and is known to contribute to the overall flavor and aroma profile of certain cultivars. Not a lot of studies have been done for this terpene. Further study is needed to understand the basics and the important roles of α-humulene (39).

2.3. Soybean Plant Nutrients

Plants require multiple nutrients to support their growth and development. Nitrogen is an essential nutrient needed by plants for various physiological processes, including seed development, root formation, and overall healthy growth (40). Nitrogen is a major component of proteins, which are crucial for plant structure and function. If there is an excessive absence or lower levels of nitrogen, plants may exhibit symptoms such as stunted growth and a light green coloring, indicating a deficiency (41-43). In addition to nitrogen, other nutrients like potassium are also essential for plant growth. Potassium plays a vital role in various plant functions, including osmoregulation, enzyme activation, and the regulation of stomatal movement. The absence or deficiency of potassium, along with other essential nutrients, can negatively impact plant growth, physical features, and internal metabolic signals (44).

When plants experience nutrient deficiencies or imbalances, they undergo internal adjustments to meet their functional demands and respond to metabolic signals for growth and reproduction. This may involve altering the composition and structure of various plant tissues, reallocating resources, or activating specific metabolic pathways to compensate for the nutrient stress (40). It is important for farmers and gardeners to ensure that plants receive an adequate supply of all essential nutrients to promote healthy growth and productivity. This can be achieved through proper soil management, including regular fertilization, and maintaining nutrient-rich soil conditions (45, 46).

Excess nitrogen and nutrients are very harmful to the plants and the environment as this can cause the plants to more attraction to insects. Nitrogen-rich plants may exhibit increased leaf and stem growth, which can attract pests and result in infestations. Balancing nitrogen levels is crucial to prevent pest problems. Excessive nitrogen availability can inhibit the formation of root

nodules in leguminous plants (45-48). These nodules house nitrogen-fixing bacteria that convert atmospheric nitrogen into a form usable by plants. Without adequate nodulation, plants rely more on external nitrogen sources, potentially leading to nutrient imbalances. Nitrogen, primarily in the form of nitrate (NO3-), can leach into the soil and contaminate groundwater through a process called nitrate leaching (49-51). Excessive nitrogen fertilization or poor management practices can result in elevated nitrate levels, which pose risks to both human health and aquatic ecosystems. Nitrate pollution is a particular concern in areas with intensive agricultural practices (40).

2.4. Background of MXenes

MXenes was first discovered by scientists at Drexel University in 2011 and represents a new family of 2D materials (52). The name "MXene" was chosen to highlight the similarity between this family of 2D materials and graphene, while also acknowledging their origin from the parent ternary carbides and nitrides known as MAX phases. MXenes are synthesized from MAX phases through a process called etching, which involves selective removal of the A element layers using chemical etchants. This etching process results in the formation of 2D MXene layers with various compositions and surface terminations, making them highly tunable (53, 54).

The discovery of MXenes has opened up exciting possibilities for exploring their unique properties and potential applications. These materials exhibit a range of interesting characteristics, including hydrophilic surfaces, high metallic conductivity, and compatibility with various chemical functionalities. MXenes have shown promise in energy storage, catalysis, water purification, and other areas, making them a rapidly growing field of study within the realm of 2D materials (53, 54).

MXenes have emerged as a significant group of 2D materials with distinct properties and numerous potential applications. MXenes are synthesized through wet-chemical etching processes using hydrofluoric acid (HF) or HF-containing etchants (55-57). This etching is necessary because the strong chemical bonds between A and M elements in MAX phases make mechanical exfoliation challenging. During the etching process, surface functionalities such as -O, -F, or -OH are introduced, denoted as T_x in the formula $M_{n+1} X_n T_x$. This etching process allows for the synthesis of MXenes with different compositions and surface terminations. Over 20 members of the MXene family have been synthesized to date, and many more are predicted, making it one of the fastest-growing families of 2D materials (55).

In comparison to other 2D materials like graphene, one notable feature of MXenes is their hydrophilic surfaces, which make them highly attractive for various applications. Additionally, MXenes exhibit high metallic conductivity, typically in the range of 6000-8000 S/cm (58-59). These properties make MXenes promising candidates for energy storage devices (60-63), water desalination (64), catalysis (65), electromagnetic interference shielding (66), transparent conducting thin films (58, 67-68), and many other applications (55).

In energy storage, MXenes have shown potential for super capacitors and batteries due to their high electrical conductivity, large surface area, and excellent ion accessibility. MXenes have also demonstrated efficient performance in water desalination processes, as their hydrophilic surfaces enable rapid ion transport and water filtration. MXenes can also be utilized to create transparent, thin films, which have applications in optoelectronics, touchscreens, and flexible electronics (55).

In 2016, MXenes were introduced to a new method called the MILD method (66, 69) which is a safer route than the direct HF method and provides a much larger and less defective

single flakes of MXenes (59). This method provides a lot of opportunities for research in the field of electronics, optical as well as has helped in improving the scale and production of MXenes.

Given the diverse properties and potential applications of MXenes, ongoing research continues to explore and develop these materials, opening up new opportunities in various fields of technology and materials science.

2.5. Different Material Characterization of MXenes and Its Importance

Characterization of MXene nanomaterials is important in nanoscience and nanotechnology as it enables researchers to understand and manipulate the properties and behavior of MXenes at a nanoscale, leading to the development of innovative application and technologies. Some of the key reasons of why MXene characterization is important:

2.5.1. Structural Determination

MXene nanomaterials often exhibit unique and complex structures and that can be studied using various characterization techniques such as SEM (21), XRD (22), and AFM (25) that allow researchers to visualize and determine the atomic or molecular arrangement, crystal structure, surface functional groups, and morphology of nanomaterials. This information is crucial for understanding the fundamental properties and structure-property relationships of MXene nanomaterials (70).

2.5.2. Size Distribution Analysis

Nanomaterials have characteristic sizes typically ranging from a few nanometers to hundreds of nanometers. Accurate measurement and control of size are vital for tailoring the properties and functionalities of nanomaterials. Characterization techniques like SEM can provide information about the size, size distribution, and shape of nanomaterials. This

knowledge is essential for optimizing synthesis methods, understanding nanoparticle growth mechanisms, and predicting material performance (70).

2.5.3. Surface Characterization

The surface of nanomaterials plays a crucial role in their properties and interactions with the environment. Techniques such as FTIR (24), and surface- enable researchers to analyze the functional groups, and surface states of nanomaterials. Surface characterization is critical for understanding surface reactivity, adsorption phenomena, and surface-related properties like catalytic activity or bioactivity (71).

2.5.4. Mechanical Characterization

MXene nanomaterials often exhibit unique properties due to their small size and high surface area. Techniques such as AFM, nanoindentation allow researchers to probe the mechanical behavior, surface topography, height retrace, and thickness of MXene nanomaterials (70). This information is crucial for designing nanomaterials for specific applications and understanding their mechanical response, for studying different mechanical properties and applications. Overall, nanomaterial characterization is critical for understanding and harnessing the unique properties of MXene nanomaterials.

2.6. Several Factors Affecting the Properties and Behavior of MXenes

MXenes are influenced by several factors that affect their properties and behavior. Here are some key factors that can significantly impact MXenes are

2.6.1. Composition

The choice of transition metals (M) and surface functional groups (X) in MXenes affects their properties. Different transition metals and surface functional groups can lead to variations

in electronic structure, chemical reactivity, surface charge, and interlayer spacing (72). The composition of MXenes determines their specific properties and potential applications.

2.6.2. Synthesis Method

MXenes can be synthesized using various methods, including etching of MAX phases, intercalation, and chemical exfoliation. The synthesis method influences the morphology, layer thickness, surface chemistry, and surface area of MXenes. Different synthesis approaches can result in variations in the structural quality, stoichiometry, and surface termination of MXenes, ultimately impacting their properties (72).

2.6.3. Intercalation and Functionalization

MXenes can undergo intercalation, where molecules or ions are inserted between the MXene layers, or functionalization, where the surface groups are modified with different chemical species. Intercalation and functionalization can alter the interlayer spacing, surface chemistry, electrical conductivity, and reactivity of MXenes (72). These modifications enable tailoring of MXene properties for specific applications.

2.6.4. Layer Thickness

MXenes can consist of few-layer or multilayer structures, and the layer thickness influences their properties. Thinner MXene layers often exhibit enhanced surface area, increased reactivity, and improved electrochemical performance (72-73). On the other hand, thicker MXene layers can provide mechanical strength and stability (73). Controlling the layer thickness allows for tuning the properties and performance of MXenes.

2.6.5. Surface Termination

The surface of MXenes is terminated by various functional groups, such as -OH, -O, or -F groups. The surface termination affects the surface charge, hydrophilicity/hydrophobicity,

interfacial interactions, and stability of MXenes (74). The choice of surface termination can impact MXene dispersion, interfacial properties, and compatibility with other materials.

2.6.6. Defects and Vacancies

MXenes can contain defects, such as vacancies, dislocations, or grain boundaries. These defects can influence the electronic properties, mechanical behavior, and catalytic activity of MXenes. The presence of defects can introduce localized states, alter charge transfer kinetics, and affect the overall performance of MXenes (72).

2.6.7. Environmental Conditions

The properties of MXenes can be influenced by the environmental conditions, including temperature (75), humidity (76), and gas atmosphere (77). MXenes can exhibit changes in structure, stability, and reactivity under different environmental conditions. Understanding the response of MXenes to environmental factors is crucial for their application in various fields, including energy storage, catalysis, and sensors (78).

By considering these factors, researchers can tailor the properties and functionality of MXenes to meet specific application requirements and explore their full potential in various fields of science and technology.

2.7. Sensing Mechanism of MXenes towards Tetraterpenes

MXenes are promising candidates for the fabrication of high-performance sensors across various wide range of applications such as healthcare diagnostics, environmental monitoring, and wearable technology. The key for developing a specific type of MXene based sensor is dependent on the different functionalization of MXene surfaces. One of the types of sensors that has been broadly studied is the development of gas sensor with high sensitivity and rapid

response that has caused a significant interest in a wide range of applications such as plant monitoring, air pollution, and biomedical applications (79).

When sensing these soybean plants that release gaseous VOCs (linalool, α-pinene, and α–humulene) during environmental stresses, these gaseous molecules are trapped by MXene sensors which exhibit an increase or decrease in the resistance (80). The cause of this resistance to change is due to the electron transfer between MXene surface layers and the terpene molecules. The main purpose of sensing these tetraterpenes using an MXene-based sensor is to do the early diagnosis of soybean plant diseases and promote healthy growth of plants.

3. MATERIALS AND METHODS

3.1. Materials

Chemicals for MXene synthesis were purchased from various sources, specifically Titanium (Ti) powder (~325 mesh, 99.5% trace metals) from Bean Town Chemical, Hudson, New Hampshire, titanium carbide (TiC) and aluminum powder (Al) (99.5% trace metal basis) from VWR, Radnor Pennsylvania, aluminum oxide (Al_2O_3) from Alfa Aesar, Haverhill, Massachusetts, ACS hydrochloric acid (HCl) (36.5-38 wt%), and lithium fluoride (LiF) (≥ 99.99% trace metals basis) from Sigma Aldrich, St. Louis, Missouri.

The plant VOC tetraterpenes are a diverse group of plant chemicals responsible for plant defense, as well as their unique aroma. They are hydrocarbons with the general formula of $C_{40}H_{56}O_2$ and are present in different forms. Several terpene-based chemicals were examined here including Linalool $C_{10}H_{18}O$ (Sigma Aldrich Product # 62139), alpha-pinene $C_{10}H_{16}$ (α-pinene, Aldrich Product # 147524), and alpha-humulene $C_{15}H_{24}$ (α-humulene, Sigma Aldrich Product # PHL83351), all of which are present in plant-based oils (6).

3.2. Preparation of MXene

The MAX phases Ti_3AlC_2 was synthesized by first ball milling TiC, Ti, and Al powders for 2 hours. The resulting powders were then pressed into a pellet and sintered at 1350 °C for 4 hours under argon flow. The collected pellets were then milled back into powder and sieved through a 160-mesh sieve. The MAX powder was then collected and stored in a small glass tube. Fluoride-based salt etchants were prepared etchant by adding 1.6 g of LiF to 15 mL of HCl and 5 mL of DI water, and then left under continuous stirring for 5 min. A total of 1.0 g of Ti_3AlC_2 powder was gradually added to the etchant above, and the reaction was allowed to run for 48 hours at room temperature of 25 ºC as shown in Figure 1.

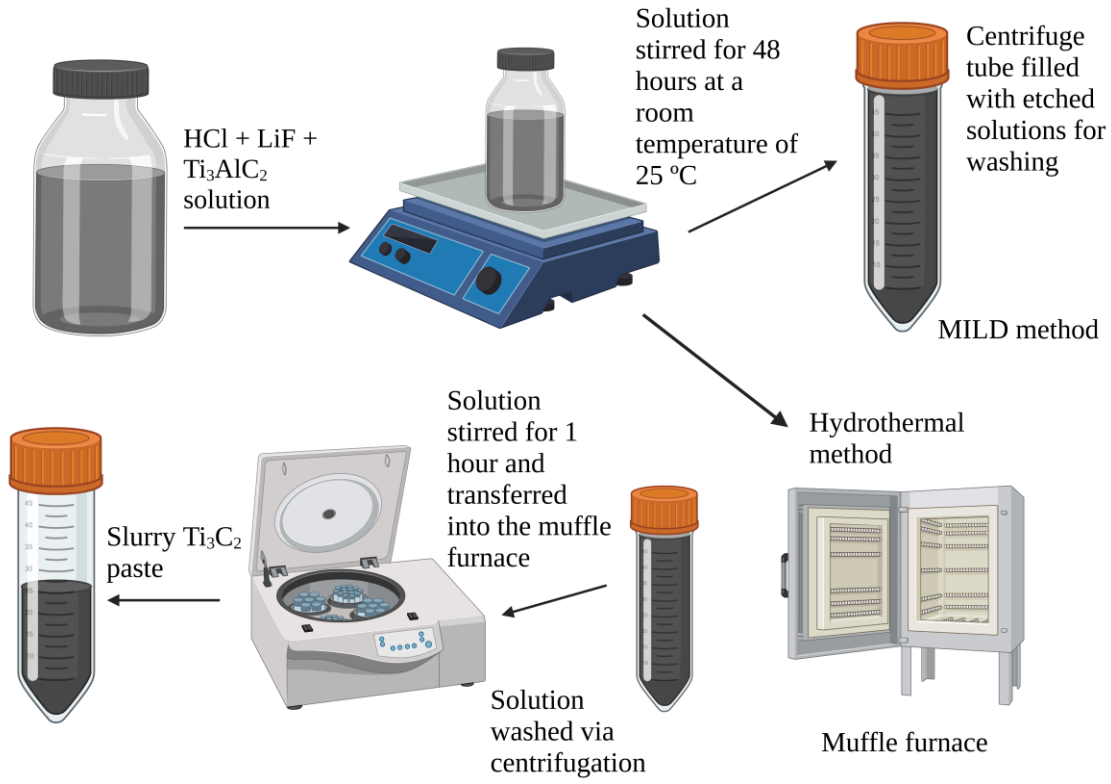

Figure 1. Schematic drawing of MXene synthesis process which included mixing HCl and LiF etchants with MAX powder, using MILD method or hydrothermal approach to etch for 48 hours at the temperature of 80 ºC, washing via centrifugation, and preparing a slurry of Ti_3C_2 MXene.

In hydrothermal approach, initially, the etchants were weighed out for LiF, HCl, and MAX using the same stoichiometric ratios and were stirred on a stir plate using a Teflon bottle at a room temperature for 1 hour. After that, the mixed solution was transferred into an autoclave and then placed in a furnace to run for 48 hours. MXene was prepared using this method at a temperature of 80 ºC. This MXene sample showed a higher purity and minimal TiC impurities. Hence, this 80 ºC MXene sample was chosen for further testing.

The etching steps were completed after 48 hours for each of the samples. During the washing process, the acidic mixtures were washed with DI water via centrifugation (5 min per 6000 rpm) for multiple cycles. The washing process continued until a pH of 4-5 was achieved.

After the washing steps were completed, the black slurry $Ti_3C_2T_x$ was collected carefully, separately from $Ti_3AlC_2/Ti_3C_2T_x$ with a spatula. These steps are summarized in Figure 1.

3.3. Coating Process of MXene

Pure MXene were coated on inter-digitated gold electrodes and were prepared to treat tetraterpenes derived chemicals (linalool, $\boldsymbol{\alpha}$-pinene, and $\boldsymbol{\alpha}$ -humulene). To prepare the slides, a small amount of Ti_3C_2 paste was transferred on inter-digitated gold electrode glass slides. The paste was uniformly applied using a single-edged cutter blade to get the desired thick film of MXene. MXene samples were coated on the slides using samples prepared at 25 ºC and 80 ºC. Once the coating process was completed, those films were dried overnight in an oven at 50 °C at a pressure ranging from 10^{-3} to 10^{-6} torr. Figure 2a shows the slides of MXene coated on an interdigitated gold electrode.

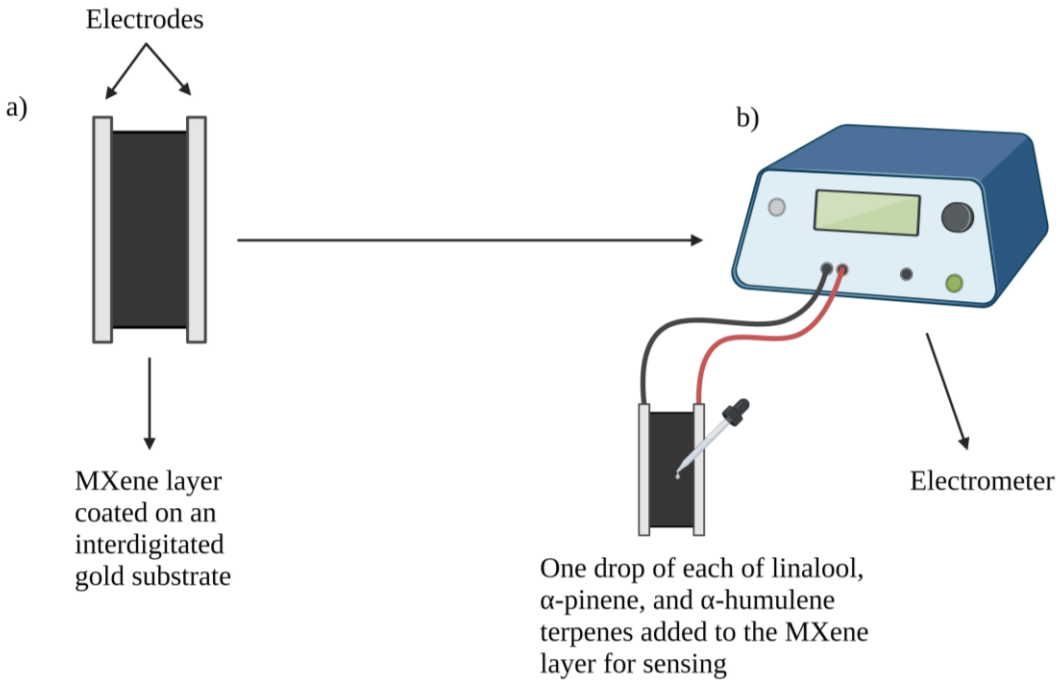

Figure 2. Experimental setup of plant sensing and detection using MXene based nanomaterial. In (a), a pure MXene coated on an interdigitated gold electrode is shown, while in (b) readings showing resistance of pure MXene samples and treated MXene samples with three different types of terpenes released from soybean plant leaves: linalool, alpha-pinene, and alpha-humulene.

3.4. Experimental Setup for Sensing Terpenes

Figure 2b shows the experimental setup of sensing and detection using this MXene based nanomaterial. The slides were connected to electrometer (Keithley multimeter) to record the initial resistance of the pure MXene samples and after treatment with the three different terpenes (linalool, alpha-pinene, and alpha-humulene). A drop of each of the terpenes (equals to 0.05ml) was added on the MXene slides using a dropper and the change in the sensitivity of MXenes recorded immediately post treatment, and for every hour for the next 24 hours. The concentration used for each of the terpenes was 1 molar (M). A standard equation was used to measure the sensitivity (S) as shown in the equation below where R_i is the initial resistance of pure untreated MXene and R_f is the resistance after treatment (81).

$$S\% = \frac{(Rf - Ri)}{Ri} * 100$$

Initially, MXenes prepared via MILD and hydrothermal methods were coated on the sensor slides and the initial resistance (R_i) was measured using an electrometer as shown in figure 2a. After that, the tetraterpenes were added to the sensing slide to montior the change in the resistance and were recorded in a data sheet. The value of R_f is the change in the resistance of the MXene sample when treated with the tetraterpenes.

Figure 3 shows an image of an inter-digitated gold electrode sensor slide. As shown in the figure, the length is 14.1 mm which is the total length (L) of the interdigitated channels, width is 1 mm which is the width (W) of each interdigitated channel, and 1 mm is the gap (G) separation between the interdigitated channels. The size dimensions of the interdigitated electrodes were measured using a vernier caliper. This sensor slide was fabricated on a glass slide with gold and patterned into an interdigitated channel. MXene samples were coated on the sensor slides and treated with tetraterpenes to measure the resistances.

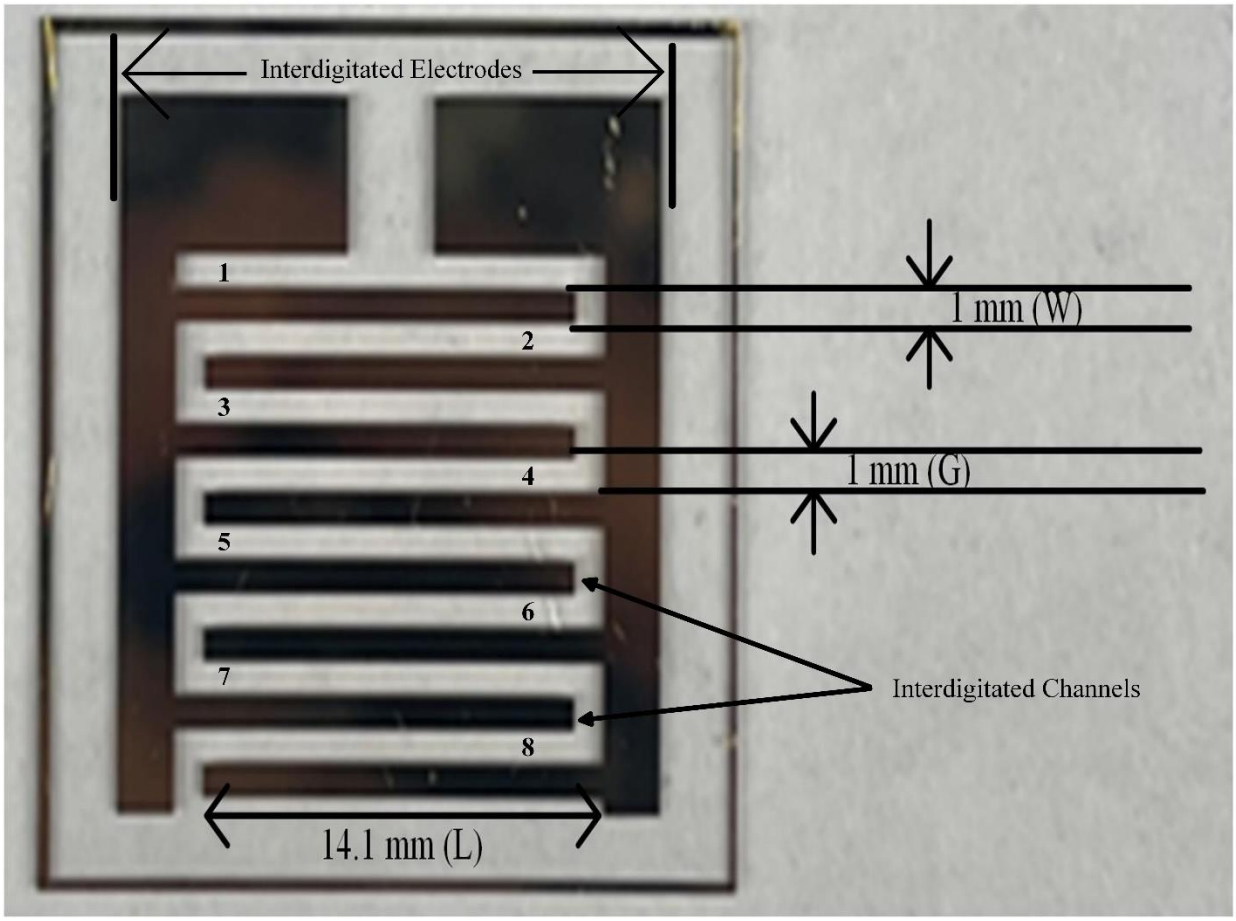

Figure 3. Schematic image of an interdigitated gold electrode sensor slides with their size dimensions of 14.1mm in length (total length of the interdigitated channels) (L), 1mm is the width (W) of each interdigitated channel and 1mm is the gap (G) separation between the two interdigitated channels. The numbers 1 through 8 indicate the number of interdigitated channels or the sections of the slide.

3.4.1. Sensing Principle of an Interdigitated Sensor Device

In order to calculate the resistance (Ω) of the thin film MXene material on the sensor slide as show in figure 3, an ohmmeter is used to get an actual reading of the MXene slide and using this resistance (Ω) along with the dimensions (thickness/trace area), the resistivity (ρ) is determined (82).

For determining the area of the interdigitated channels, it is calculated through finding the relative surface areas of the intermediary space between the gold contacts and adding those up all

together to find the total surface area of the plane. The thickness (or the height) of the MXene film is what is important when using the given equation below (82).

$$\text{Resistance } (\Omega) = \text{Resistivity } (\rho) * \frac{\text{Thickness of MXene film}}{\text{Area of intermediary space}}$$

For measuring the surface area of the interdigitated electrodes:

$$\text{Surface area (A)} = [14.1\text{mm} \times 1\text{mm}] \times 8 \text{ sections} = 116 \text{ mm}^2$$

$$= [1\text{mm} \times 1\text{mm}] \times 8 \text{ sections} = 8 \text{ mm}^2$$

$$\text{Total Surface Area} = 124 \text{ mm}^2 = 1.24 \text{ cm}^2$$

The measurement was done using a vernier caliper where 14.1 mm indicates the total length of the interdigitated channels (L) and is multiplied by the width of each interdigitated channel (1mm) (W) times the total number of sections (channels) which is 8 in the slide as shown in figure 3.

3.4.2. Mechanism of the Flow of Current in an Interdigitated Electrode and Its Effect on the Resistance

As shown in figure 3, when the electric probes are connected to the slide, a constant current is applied to the interdigitated electrodes by connecting a voltage source across the electrodes. The current flows through the electrodes, passing through the gaps (G) between the channels. For measuring the resistance using an ohmmeter, when there is no conductive material present in the gaps (G) between the channels, the current flows freely through the gaps (G), resulting in low resistance. However, when a conductive material like MXene is placed on or in proximity to the interdigitated electrodes, it bridges the gaps (G), creating a pathway for the current which leads to an increase in the resistance (82).

3.4.3. Factors Affecting the Readings of Resistance of an Interdigitated Electrode

3.4.3.1. Length of the Interdigitated Channels

The length of the electrodes affects the total resistance of the interdigitated electrodes structure. The resistance of the interdigitated electrodes is directly proportional to the length of the electrodes. A longer electrode length results in higher resistance, while a shorter length leads to lower resistance. This relationship can be understood by considering the geometry of the interdigitated electrodes. Longer electrodes offer a longer path for the current to flow through, increasing the overall resistance. Conversely, shorter electrodes provide a shorter path, reducing the resistance (83).

3.4.3.2. Width of the Interdigitated Channels

The resistance between the interdigitated electrodes is inversely proportional to the width of the electrodes. A narrower width results in higher resistance, while a wider width leads to lower resistance. This relationship can be understood by considering the geometry of the interdigitated electrodes. A narrower electrode width restricts the current flow, increasing the resistance. Conversely, a wider electrode width allows for more current to pass through, reducing the resistance (83).

3.4.3.3. Thickness of MXene Films

The resistance of the interdigitated electrodes is indirectly influenced by the thickness of MXenes coated on an interdigitated electrode. Thicker MXene materials generally have lower resistance compared to thinner MXene materials. This relationship occurs because thicker MXenes offer a lower resistivity path for the current to flow through, resulting in reduced resistance. However, it's important to note that the effect of thickness on resistance is relatively minor compared to other factors like width (W) and gap (G) (83).

3.5. Material Characterization

Several material characterization tests were performed on pure untreated and post-treated samples to study the overall morphology of pure MXene, and changes caused by terpenes treatment to identify the underlying mechanics of MXene sensing. These included structure analyses using FE-SEM using JSM-7600F (JEOL, USA), crystal structure via XRD using D8 DISCOVER (Bruker, USA), and chemical composition and surface functional group analysis via Vertex 70 FTIR spectrometer Bruker Optics using OPUS^{TM} and OPUSLab^{TM} software. Similarly, using AFM to study the surface roughness of the MXene samples using Jupiter XR; Asylum Research AFM Oxford Instrument and the software used was Blue Drive AC Air Topography/Jupiter 18.20.38/ Igor Pro 6.38B01.

The FE-SEM and AFM provided the overall morphology and surface roughness of pure MXene samples. The XRD was measured from 2-theta values of 5° to 75° to examine the crystal structure for studying the purity of the MXene sample and to look for its changes post-treatment. ATR-FTR uses light-based methods to examine the molecular composition and functional groups for pure and treated MXene material. The ATR-FTIR signature was measured 500 to 4500 cm^{-1} to identify the functional groups involved on the surface layers of pure MXene samples.

4. RESULTS AND DISCUSSION

4.1. Structural Characterization of MXene Samples

Figure 4 shows the FE-SEM of typical structure observed for MXene samples prepared by the MILD (room temperature of 25 °C) (figure 4a) and the hydrothermal approach (heated at a temperature of 80 °C) (figure 4b) to study the overall morphology. The MXenes were all observed to be single layered structure. For sample prepared using MILD (figure 4a), the flake sizes were minimal and present in small traces under the magnification of 20,000x. In contrast, for sample prepared using hydrothermal approach, a single layer of large flakes with distinct and sharp edges were observed (figure 4b) under a magnification of only 6200x. This shows that MXenes flakes are large even under lower magnification. Earlier literature has reported similar results of receiving higher purity of the MXene using a hydrothermal method (84, 85). From the FESEM, it can also be observed that MXene's edges had a rougher surface, showing that the when MXene samples are etched at a higher temperature, it affects the produced material.

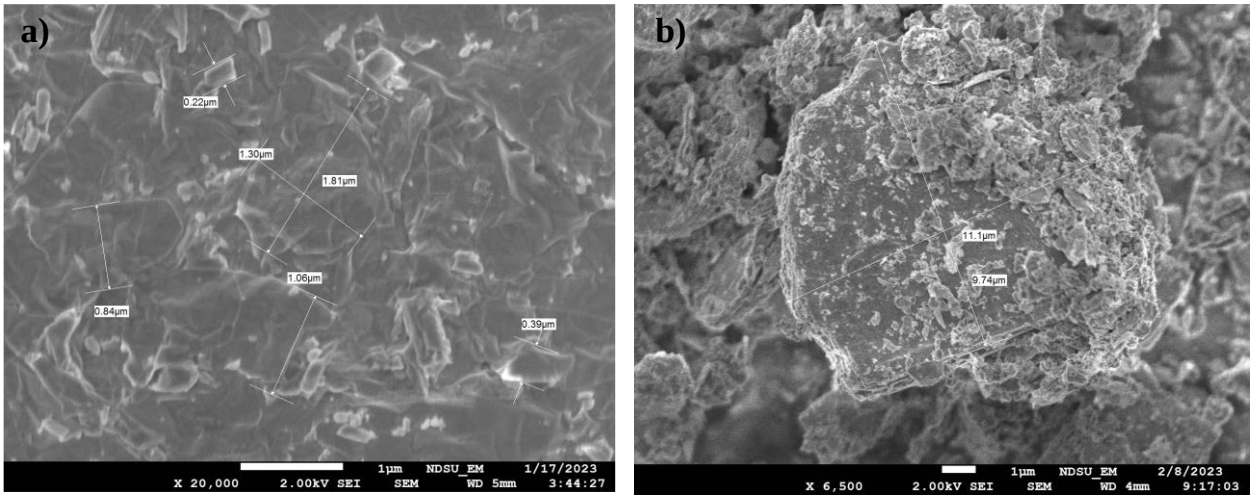

Figure 4. Typical SEM images of pure untreated MXene samples synthesized using (a) the MILD method in which the stirring occurred at a temperature of 25 ºC (b) the hydrothermal method where post stirring processing included high temperature storage at 80 ºC and solution washing. The flake size distribution for MILD was 1.81µm by 1.30µm and for hydrothermal processing was 11.1µm by 9.74µm.

Samples etched with an HCl/LiF solution show few mono layered MXene sheets have been reported due to Li+ ion intercalation between nanosheets which weakens any electrostatic interaction that holds them together (86). MXene sheets can be seen to be formed in each sample, which is further shown by XRD later on. Sample prepared via MILD method show mostly impurities on the surface of the material and around. The sample grown at 80 °C (figure 4b), however, shows good morphology and single sheet material can be seen residing on the substrate as small translucent flakes around the larger few-layered sheet in the center. This is evidence that growth at 80 °C etched with HCl/LiF solution using the hydrothermal route showed the best under the observed experimental conditions.

Overall, the FESEM data shows that we can successfully etch $Ti_3C_2T_x$ MXenes at high temperature from the Ti_3AlC_2 MAX phase, and that increasing the etching temperature makes much more impactful to the final MXene material's morphology. We can also gather from this data that tuning the temperature conditions could allow for the control over the final material's layer spacing when using the hydrothermal method. Using the hydrothermal method, we see indications of a higher purity sample when etched at 80 °C, with minimal impurity present in the sample. Purity will be further discussed when studying XRD.

4.2. Crystal Structure Characterization via XRD

XRD was used to study the $Ti_3C_2T_x$ MXene's crystal structure and purity. Figure 5 shows typical XRD peaks for MXenes prepared using different approaches. In the hydrothermal method, the *(002)* peak is the MXene peak at 7.087°. Also, the peaks *(004)* indicate the MXene peak at 14.311° whereas *(006)* indicate the Li_3AlF_6 at 28.851°. In MILD method, the *(002)* peak intensity is very weak and shows the presence of TiC impurities at 35.985° and 44.96° which is indicated by *(008)* and *(0012)* and for Ti_3AlC_2 by *(0010)* at 38.715° and 41.835° (85, 86).

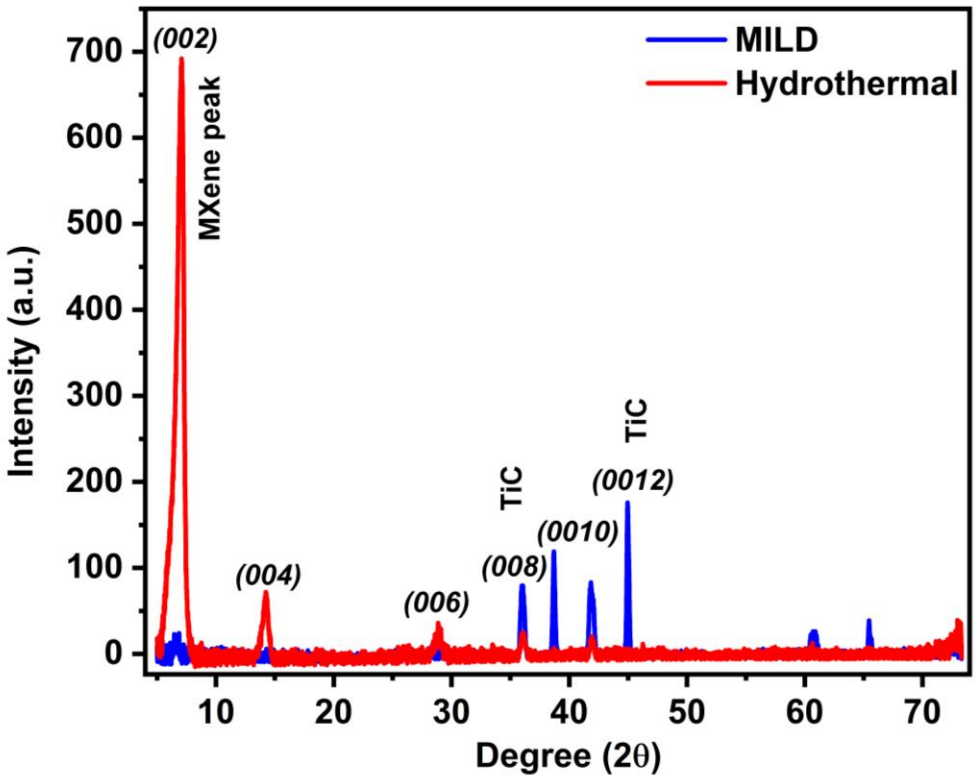

Figure 5. XRD patterns of MXene samples synthesized using MILD and hydrothermal method. The *(002)*, *(004)*, and *(006)* peaks represent the MXene peaks whereas the peaks *(008)* and *(0012)* represent TiC impurities and for Ti_3AlC_2 MAX *(0010)* peak respectively.

In the hydrothermal method, the *(006)* peak has been attributed to Li_3AlF_6 which has formed over the course of the experiment and is likely the debris seen in the SEM results mentioned earlier. Also, in good agreement with SEM, it can be seen that the sample grown at 80 °C (hydrothermal) has the most prominent characteristic MXene peak indicating that this sample likely has the highest quality of MXenes present. Combining this with the SEM data, we can surmise that samples grown up to 80 °C (hydrothermal) increase purity due to a more thorough etching process, but at 25 °C (MILD) decrease in quality is seen due to different etching conditions.

The MXene sample synthesized using MILD method showed no presence of the prominent *(002)* peak and instead showed the presence of Al and TiC impurities, which indicates

that the MAX layer was not etched out completely. In comparison, hydrothermal processed MXene peak is prominently present with minimal traces of Al and TiC peaks, which indicates that Al was completely etched out from the MXene layer and was replaced by the -OH groups which are the surface terminating groups at the MXene surface region (86).

From the XRD results, it can be stated that MXene synthesized using hydrothermal method showed better outcome of etching out the MAX phase and resulting in higher purity of the MXene samples. In comparison, the MXene prepared by MILD method showed minimal peak for MXene and presence of TiC impurities which indicated that the sample was not highly pure.

4.3. Surface Group Analysis via FT-IR

ATR-FTIR was performed to study the surface functional groups of MXene samples. Figure 6 shows the ATR-FTIR of pure MXene samples used for identifying the functional groups involved on the surface layer of MXenes.

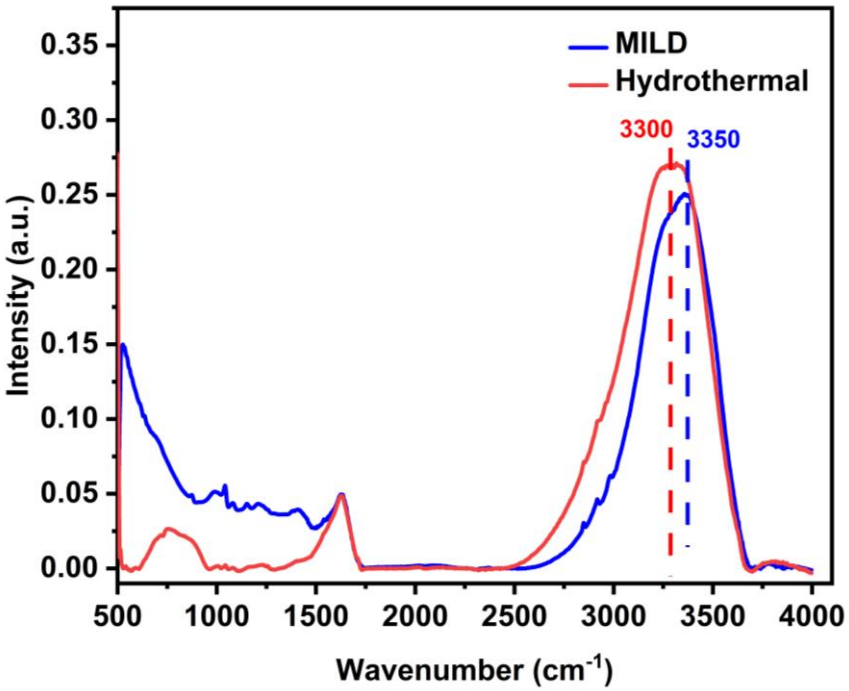

Figure 6. FTIR-ATR Spectroscopy of pure MXene sample with wave number ranging from 500-4000/cm using MILD and hydrothermal method. Both methods show the presence of –OH groups at about 3300/cm-3350/cm on MXene surface layers which indicates that MXene are hydrophilic.

As shown in figure 6, it can be seen that the -OH groups are the strongest and have a broad range at about 3300/cm. There are carbon and hydrogen bonds C-H detected but are shown to be weak at a range of 1650/cm. It shows that the MILD method MXene sample has -OH groups on the surface layers of MXene. Similarly, the hydrothermal method shows a strong and broad peak of -OH groups as well as the C-H bending at about a range of 1650/cm. MXene surface functionalization was changed when the sample was synthesized using hydrothermal compared to MILD method. From the results, it can be confirmed that the -OH groups exist in both MILD and hydrothermal MXene surface layers. Overall, from the ATR, it can be confirmed that all the pure MXene samples have -OH groups present on the surface layers making it hydrophilic. However, due to the difference in the synthesis methods led to the change in the intensity of those -OH groups involved on the MXene surface layers.

4.4. Surface Roughness Characterization Using AFM for MXene Modified With Tetraterpenes

AFM was performed to study the overall surface roughness of the MXene samples treated with tetraterpenes. Typical AFM image with a scan size of 20µm were collected for MXene using MILD and hydrothermal method as shown in figure 7.

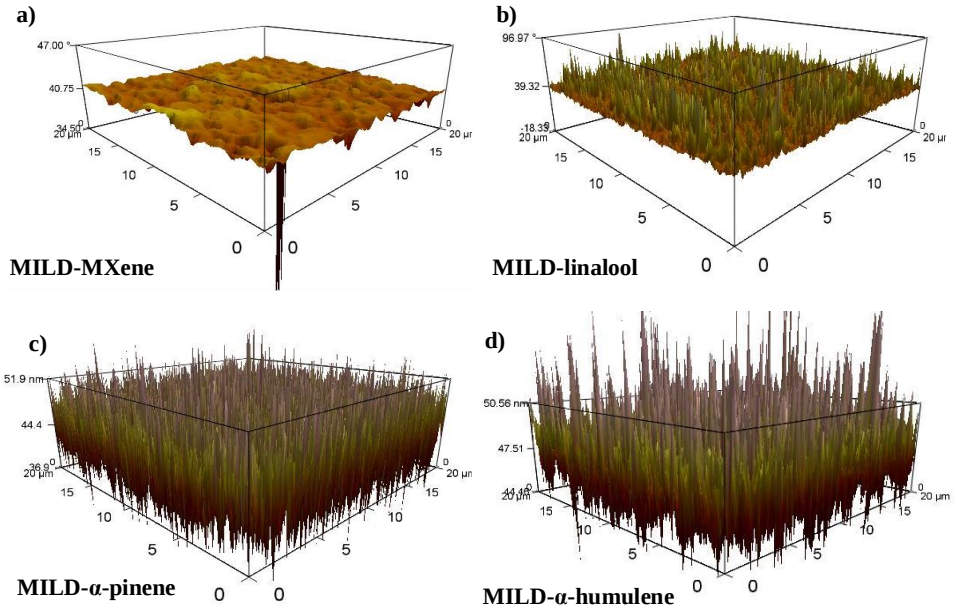

Figure 7. Comparison of AFM images of pure MXene sample using different etching routes (a) MILD (25 °C) and (b) hydrothermal (80 °C) method. AFM images of MXene samples treated using tetraterpenes (c) MILD + linalool (d) MILD + alpha-pinene (e) MILD + alpha-humulene (f) hydrothermal + linalool (g) hydrothermal + alpha-pinene (h) hydrothermal + alpha-humulene (i) hydrothermal (30 °C) + DI water (j) hydrothermal (30 °C) + toluene (k) hydrothermal (60 °C) + toluene. All images show the comparison of surface roughness using the same magnification of 20µm.

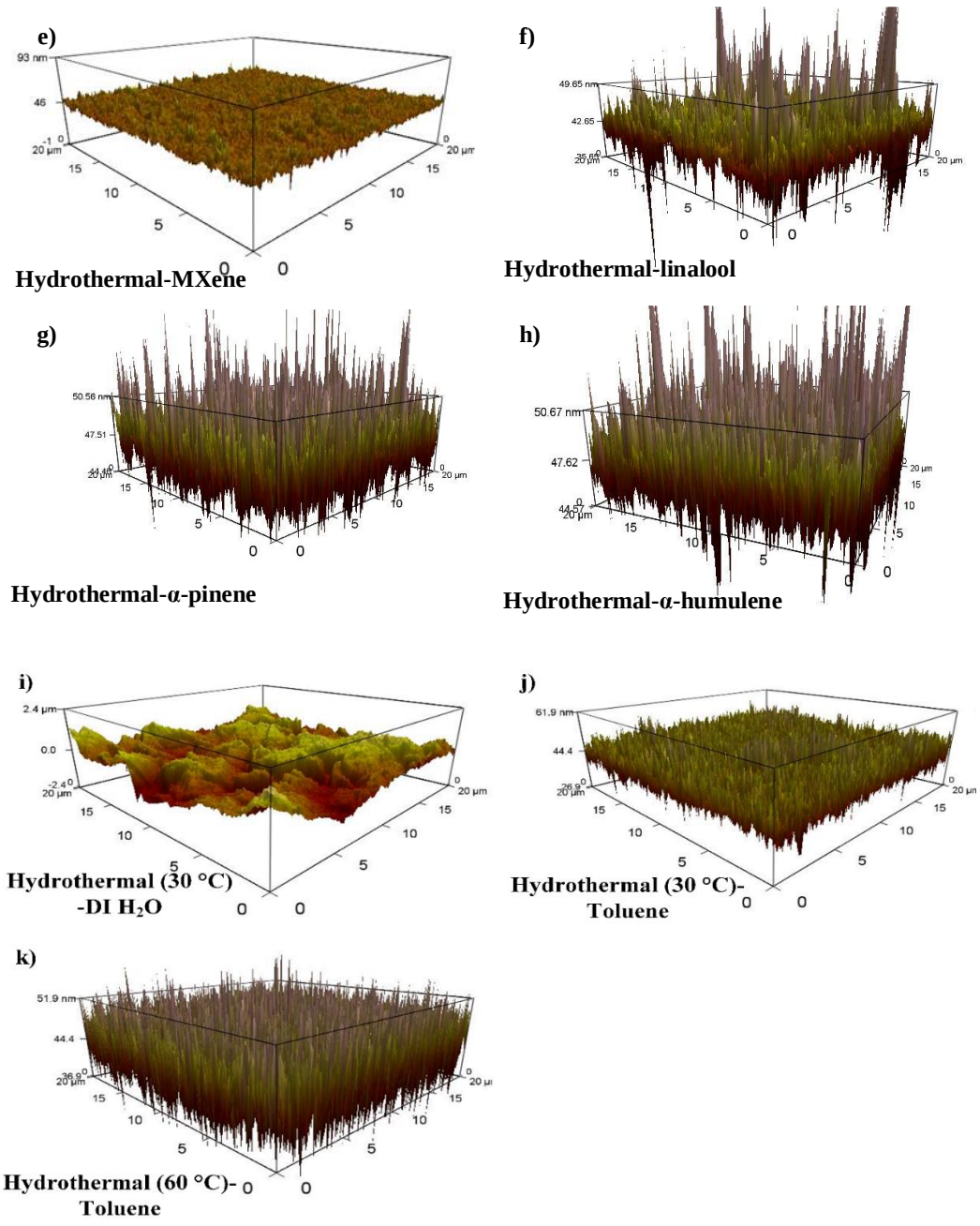

Figure 7. Comparison of AFM images of pure MXene sample using different etching routes (a) MILD (25 °C) and (b) hydrothermal (80 °C) method. AFM images of MXene samples treated using tetraterpenes (c) MILD + linalool (d) MILD + alpha-pinene (e) MILD + alpha-humulene (f) hydrothermal + linalool (g) hydrothermal + alpha-pinene (h) hydrothermal + alpha-humulene (i) hydrothermal (30 °C) + DI water (j) hydrothermal (30 °C) + toluene (k) hydrothermal (60 °C) + toluene. All images show the comparison of surface roughness using the same magnification of 20µm.(continued)

The image modes for MILD method (figure 7a) were setup at a setpoint of 925.21mV, drive amplitude of 5.13mW, drive frequency of 69.745 kHz, and integral gain of 111.22. Similarly, for hydrothermal method (figure 7b) were setup at a setpoint of 945.70mV, drive amplitude of 4.87mW, drive frequency of 69.745 kHz, and integral gain of 32.49.

As shown in figure 7 (c) through (e) MXene using MILD method (25 °C) treated with tetraterpenes showed a significant change in the surface roughness. The surface looked smoother before the treatment (as shown in figure 7a). However, the surface looked completely deformed after treating the MXene using MILD with the tetraterpenes as shown in figure 7 (c) through (e). Similarly, in figure 7 (f) though (h) shows similar change in the surface layer when MXene using hydrothermal method (80 °C) were treated with tetraterpenes. The MXene surface layer showed a complete deformation after the treatment with tetraterpenes which indicates that the tetraterpenes had a significant response on the surface layers of MXene using both MILD and hydrothermal method.

Conversely, MXene synthesized at 25 °C and 80 °C using hydrothermal method were treated with DI water and toluene. In the case of DI water, which is a polar molecule, did not show much of a change in the structure whereas in toluene which is a nonpolar solvent showed similar changes in the morphology like the tetraterpenes as shown in Fig. 7 (i) through (k). These comparisons were performed to see if the polar or the nonpolar molecules have any significant effect on the MXene surface layers. In fact, MXenes synthesized under different conditions (MILD and hydrothermal) had a significant change in the morphology when treated with linalool, alpha-pinene, and alpha-humulene which are all nonpolar molecules. Whereas MXene with DI water did not have any effect in morphology, that means the polar molecules like the DI water do not show any effect when it is treated on MXenes. In the case of toluene,

MXene at 25 °C and 80 °C using hydrothermal had a significant change on the surface layer. Overall, it shows that MXenes using MILD and hydrothermal method shows changes in the morphology when using nonpolar molecules whereas with polar molecules like the DI water had no impact on the morphology. The reason is still under investigation.

4.5. MXene Response to Tetraterpenes

As stated earlier, we examined MXene response in the presence of several terpene-based chemicals including, linalool, α-pinene, and α-humulene with data taken every hour for 12 hours. Figure 8 shows the typical data for tetraterpenes-treated MXene samples synthesized using MILD method.

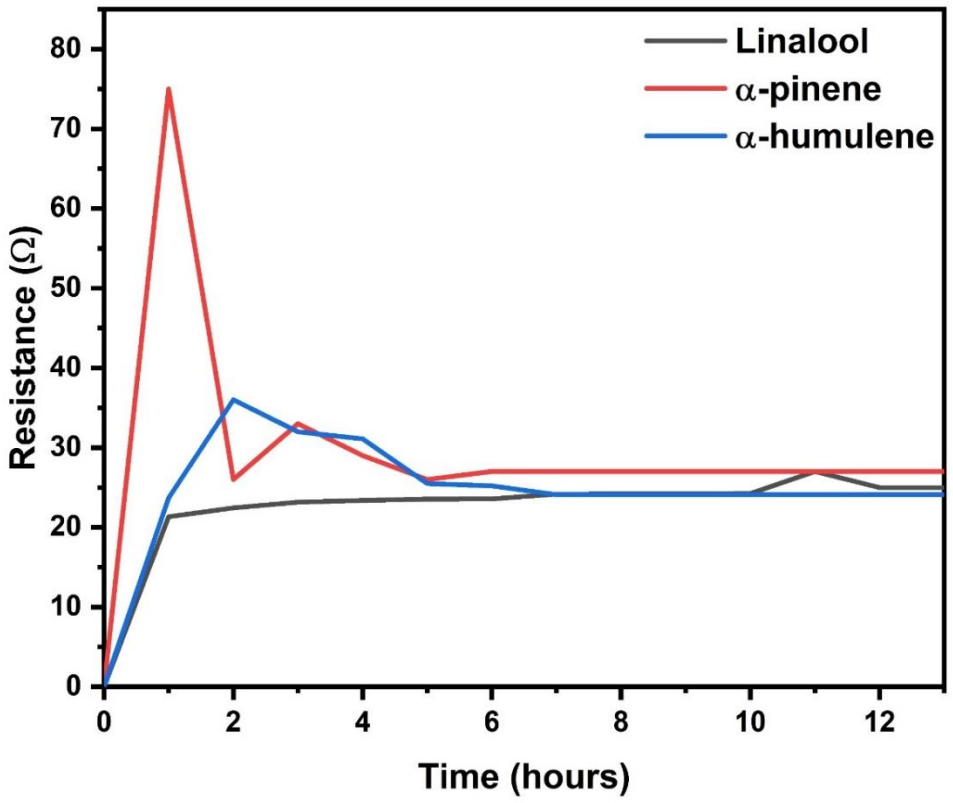

Figure 8. Resistivity of treated terpenes on MXene sample synthesized through MILD method. Alpha-pinene shows the most significant response in the first few hours compared to linalool and alpha-humulene but later had a stable range of resistance as the number of hours were increased during the treatment with terpenes.

It is shown that the resistivity of MXene samples changes with and is directly affected by the type of tetraterpenes. Specifically, alpha-pinene had the most significant effect on MXene that first led to the increase in resistance to 75Ω and decreased and became stable to around 28 Ω after 5 hours. The linalool and alpha-humulene samples had a similar response with time MXene with stabilized values of 21Ω and 36Ω respectively but changes were not as significant as alpha-pinene.

Table 1 gives a summary of the MXenes samples prepared using MILD (S1) and hydrothermal (S2) routes and the resistance measured before (b) and after (a) the treatment with tetraterpenes along with its dimensions (length, width, and thickness) in millimeter (mm) of the MXene sensor slides.

Table 1. MXene samples prepared via MILD (S1) and hydrothermal (S2) routes along with their dimensions and resistance before (a) and after (b) the treatment with tetraterpenes.

Material Conditions	Tetraterpenes	Dimensions (mm)	Resistance (Ω)
S1: 25 ºC (MILD)	Linalool	14.1 x 1 x 0.0144	22^{b} Ω
			27^{a} Ω
	Alpha-pinene	14.1 x 1 x 0.0256	75^{b} Ω
			33^{a} Ω
	Alpha-humulene	14.1 x 1 x 0.0185	24^{b} Ω
			36^{a} Ω
S2: 80 ºC (Hydrothermal)	Linalool	14.1 x 1 x 0.0119	1.02^{b} Ω
			1.02^{a} Ω
	Alpha-pinene	14.1 x 1 x 0.0213	1.55^{b} Ω
			1.83^{a} Ω
	Alpha-humulene	14.1 x 1 x 0.0237	1.69^{b} Ω
			35.5^{a} Ω

As shown in table 1, when linalool terpene was treated on the MXene sensor slide, it can be seen that the difference in resistance was 5Ω under MILD condition and 0.13Ω under hydrothermal condition. Similarly, for α-pinene terpene, the difference in the resistance was 42Ω

and 0.28Ω under MILD and hydrothermal conditions. In the case of α-humulene, the change in resistance was 12Ω and 33.81Ω under both conditions. One of the reasons for this change to occur is due to the MXene samples that were prepared under different conditions which influences the morphology, surface chemistry, and surface area of MXenes. Different synthesis approaches can result in variations in the overall structural quality, stoichiometry, and surface termination of MXenes, ultimately impacting their properties (72). The other reason for this change is due to the difference in the thickness of MXene samples. The samples used during the testing with terpenes were mostly thin MXene layers. There were changes seen in the resistance and this is due to the effect of difference in the thickness of the MXene layers. From a literature review, it was stated that thinner MXene often exhibits enhanced surface area, increased reactivity, and improved electrochemical performance (72-73). On the other hand, thicker MXene layers can provide mechanical strength and stability (73).

Table 2 provides a summary of the percentage of sensitivity of MXenes treated with terpenes. The sensing response was measured by a standard equation called the sensitivity (S) as shown in the equation below where R_i is the initial resistance of pure untreated MXene and R_f is the resistance after treatment (81).

$$S\% = \frac{(Rf - Ri)}{Ri} * 100$$

Table 2. MXene samples using MILD and hydrothermal routes and their sensing response towards tetraterpenes.

Material Conditions	Linalool	α-pinene	α-humulene
25 ºC (MILD)	26.6%	56.0%	51.9%
80 ºC (Hydrothermal)	12.7%	18.3%	>100%

It can be observed that the MXene using MILD and hydrothermal methods had interactions with linalool, alpha-pinene, and alpha-humulene. MXenes treated with alpha-pinene

and alpha-humulene had greater sensing response as compared to linalool. Also, table 1 shows the sensitivity performance using hydrothermal route in which alpha-humulene had the greatest sensitivity performance in comparison to linalool and alpha-pinene.

This change in the sensitivity performance is expected to be due to the surface layer of MXene material which has mostly –OH groups as confirmed by ATR outcomes shown in figure 6 using MILD method. In linalool, the –OH group is present in the molecular structure and MXene has –OH groups on the surface layers. When the linalool was treated with sample of MXene using MILD, their interaction was minimal due to their similar charges. Both the MXene and linalool had negative charges from the –OH groups that led to repelling from one another. So, the sensing performance was not strong enough for linalool and that led to only 27% for MXene. In case of alpha-pinene, there are two types of isomers: –cis and –trans pinene (84, 87). In –cis type of pinene, it has mostly positive charges whereas in –trans it has negative charges. From the table 1, it was confirmed that the alpha-pinene were most likely a –cis type because the MXene surface layers with -OH groups had a strong interaction with the positive charges of pinene which led to the significant increase in the sensitivity performance. Similarly, in alpha-humulene, it has a strong dipole-dipole interaction (85). It means that the positive and negative interaction between the humulene molecules and MXene surface layer –OH groups led to a strong bonding between them. That is why the sensitivity was significant for MXene treated with alpha-humulene. Overall, it can be stated that the change in the MXene surface chemistry led to the difference in the sensitivity of the treated MXenes.

The response of the MXene response to plant chemical tetraterpenes prepared using the two methods was shown in table 1 which includes direct use of tetraterpenes drops on the MXene samples to check for its conductivity.

From the results, it was shown that MXene treated with linalool had a weaker interaction with the MXene surface layer molecules whereas alpha-pinene and alpha-humulene had the strongest dipole-dipole interaction with these MXene surface layer FESEM images were obtained of pure MXenes samples and showed a change in the morphology/structure of MXene surface layers. XRD was also performed for pure MXene samples and showed that the hydrothermal route has a higher purity compared to MILD. Further analyses were performed using FTIR-ATR where the MXene surface functional groups were studied in which –OH groups were successfully detected for all pure MXene samples. Overall, it can be concluded that the plant nutritional stresses that are tetraterpenes have a direct impact on the surface chemistry of MXene. This has opened up a way for treating plant bacterial diseases beforehand and to prevent any sort of growth of plant diseases.

The sensor characterization showed that the MXene surface layer with –OH groups bonded with the tetraterpenes positive and negative charges present on the molecular structure showing a significant sensitivity response for all terpenes. However, as shown in figure 6, there was a significant response only for terpene alpha-pinene and alpha-humulene using MILD route MXene sample whereas for linalool terpene was minimal. In linalool terpene, the decrease in the sensitivity performance is due to the repulsion between the negative -OH group in the molecular structure and the MXene surface layer. However, for alpha-pinene, they are most likely a –cis type of isomer which have positive charges and the MXene surface layer with –OH groups had a strong interaction with the positive charges of pinene which led to a significant increase in the sensitivity performance. Similarly, in case of alpha-humulene, the presence of positive charge group in humulene led to a strong interaction with the negative –OH surface functional group of MXene layer.

5. LIMITATIONS, CHALLENGES, FUTURE DIRECTIONS, AND CONCLUSION

There are certain limitations in this study while using hydrothermal routes for MXene synthesis. Temperatures of 30 ºC and 60 ºC did not work for the sensing with terpenes as the samples were not stable and had mostly impurities. However, for 80 ºC the samples synthesized were highly pure, stable, and gave significant responses in resistivity when treated with terpenes.

There are certain significant challenges in plant growth and one of them is the impact of environmental stresses on the plants that are sensitive, resulting in lower crop yields. So, understanding the mechanism and rate of plant growth under the influence of environmental conditions is an important step towards precision farming, which ensures effective growth and viable use of resources. Beyond addressing the challenges, the sensor application for plant health growth and monitoring with increase in the demand in precision agriculture for addressing challenges of food and water insecurity under high environmental changes. There are studies that show that the plants are exposed to stresses both from the bacteria and pathogens (biotic) and environment (abiotic) during the growth stages (88-90). Also, studies show the relationship between the plant volatile organic compounds (VOCs) emission and environmental stressors to address different functions such as defense, pollution, and bio-signaling (4, 91-93). Thus, designing of a new VOC sensor for selectively sensing gases and VOCs in plants is another important way reported by earlier research groups (93, 94). Similarly, developing a higher quality of MXene and its high capacity for surface functionalization for targeted applications can be studied in the plant sensing field (95, 96).

In summary, in this study, we developed and characterized a reasonable MXene/gold interdigitated electrode sensor and demonstrated its use to detect the tetraterpenes released by the

soybean plant leaves. MXene samples were synthesized using two different routes MILD and hydrothermal and then were tested with different terpenes to reveal the sensitivity of MXenes. In conclusion, based on our experiments experimental, the key outcomes can be summarized below:

1. A sensor was fabricated by using drop cast technique to coat MXene on a gold-interdigitated electrode.
2. From the results, we have found that the terpenes have a direct effect on the surface chemistry of MXene samples.
3. The MXene surface layer with -OH groups had a direct interaction with the positive and negative charges of terpenes present on the molecular structure.

Overall, our study demonstrated the application and the sustainability of our low-cost stress sensor for monitoring plant growth. The easy synthesis of MXene and the use of gold substrate provides a new way of developing affordable plant sensing device. It provides a new way to develop plant strain sensors for precision agriculture, with many future opportunities for plant sensing application and a new sensor development. It can be concluded that the plant nutritional stresses that are tetraterpenes have a direct effect on the resistance for all MXene samples made. This has opened up a way for treating plant bacterial diseases beforehand and preventing any sort of growth of plant diseases.

REFERENCES

1. Borode T, Wang D, Prasad A. Polyaniline-based sensor for real-time plant growth monitoring. Sensors and Actuators A: Physical. 2023 Jun 1;355:114319.

2. Savary S, Ficke A, Aubertot JN, Hollier C. Crop losses due to diseases and their implications for global food production losses and food security. Food security. 2012 Dec;4(4):519-37.

3. Stein EW. The transformative environmental effects large-scale indoor farming may have on air, water, and soil. Air, Soil and Water Research. 2021 Mar;14:1178622121995819.

4. Roy M, Prasad A. Raman spectroscopy for nutritional stress detection in plant vascular tissue. Materialia. 2022 Aug 1;24:101474.

5. Robertson GP, Vitousek PM. Nitrogen in agriculture: balancing the cost of an essential resource. Annual review of environment and resources. 2009 Nov 21;34:97-125.

6. Sofowora A, Ogunbodede E, Onayade A. The role and place of medicinal plants in the strategies for disease prevention. African journal of traditional, complementary and alternative medicines. 2013 Aug 14;10(5):210-29.

7. Soleymaniha M, Shahbazi MA, Rafieerad AR, Maleki A, Amiri A. Promoting role of MXene nanosheets in biomedical sciences: therapeutic and biosensing innovations. Advanced healthcare materials. 2019 Jan;8(1):1801137.

8. Mazari SA, Ali E, Abro R, Khan FS, Ahmed I, Ahmed M, Nizamuddin S, Siddiqui TH, Hossain N, Mubarak NM, Shah A. Nanomaterials: Applications, waste-handling, environmental toxicities, and future challenges–A review. Journal of Environmental Chemical Engineering. 2021 Apr 1;9(2):105028.

9. Bhardwaj R, Hazra A. MXene-based gas sensors. Journal of Materials Chemistry C. 2021;9(44):15735-54.

10. Xiao B, Li YC, Yu XF, Cheng JB. MXenes: Reusable materials for NH3 sensor or capturer by controlling the charge injection. Sensors and Actuators B: Chemical. 2016 Nov 1;235:103-9.

11. Zhou L, Zhang X, Ma L, Gao J, Jiang Y. Acetylcholinesterase/chitosan-transition metal carbides nanocomposites-based biosensor for the organophosphate pesticides detection. Biochemical Engineering Journal. 2017 Dec 15;128:243-9.

12. Wu M, He Y, Wang L, Xia Q, Zhou A. Synthesis and electrochemical properties of V 2 C MXene by etching in opened/closed environments. Journal of Advanced Ceramics. 2020 Dec;9:749-58.

13. Anasori B, Lukatskaya MR, Gogotsi Y. 2D metal carbides and nitrides (MXenes) for energy storage. Nature Reviews Materials. 2017 Jan 17;2(2):1-7.

14. Ling Z, Ren CE, Zhao MQ, Yang J, Giammarco JM, Qiu J, Barsoum MW, Gogotsi Y. Flexible and conductive MXene films and nanocomposites with high capacitance. Proceedings of the National Academy of Sciences. 2014 Nov 25;111(47):16676-81.

15. Luo J, Tao X, Zhang J, Xia Y, Huang H, Zhang L, Gan Y, Liang C, Zhang W. Sn4+ ion decorated highly conductive Ti3C2 MXene: promising lithium-ion anodes with enhanced volumetric capacity and cyclic performance. ACS nano. 2016 Feb 23;10(2):2491-9.

16. Zhang M, Cao J, Wang Y, Song J, Jiang T, Zhang Y, Si W, Li X, Meng B, Wen G. Electrolyte-mediated dense integration of graphene-MXene films for high volumetric capacitance flexible supercapacitors. Nano Research. 2021 Mar;14:699-706.

17. Alnoor H, Elsukova A, Palisaitis J, Persson I, Tseng EN, Lu J, Hultman L, Persson PÅ. Exploring MXenes and their MAX phase precursors by electron microscopy. Materials Today Advances. 2021 Mar 1;9:100123.

18. Kvashina TS, Uvarov NF, Korchagin MA, Krutskiy YL, Ukhina AV. Synthesis of MXene Ti3C2 by selective etching of MAX-phase Ti3AlC2. Materials Today: Proceedings. 2020 Jan 1;31:592-4.

19. Peng C, Wei P, Chen X, Zhang Y, Zhu F, Cao Y, Wang H, Yu H, Peng F. A hydrothermal etching route to synthesis of 2D MXene (Ti3C2, Nb2C): Enhanced exfoliation and improved adsorption performance. Ceramics International. 2018 Oct 15;44(15):18886-93.

20. Wu M, He Y, Wang L, Xia Q, Zhou A. Synthesis and electrochemical properties of V 2 C MXene by etching in opened/closed environments. Journal of Advanced Ceramics. 2020 Dec;9:749-58.

21. Alyamani AM, Lemine OM. FE-SEM characterization of some nanomaterial. InScanning electron microscopy 2012 Mar 9. IntechOpen.

22. Holder CF, Schaak RE. Tutorial on powder X-ray diffraction for characterizing nanoscale materials. Acs Nano. 2019 Jul 23;13(7):7359-65.

23. Coury C, Dillner AM. ATR-FTIR characterization of organic functional groups and inorganic ions in ambient aerosols at a rural site. Atmospheric Environment. 2009 Feb 1;43(4):940-8.

24. Yang L, Wen KS, Ruan X, Zhao YX, Wei F, Wang Q. Response of plant secondary metabolites to environmental factors. Molecules. 2018 Mar 27;23(4):762.

25. Binnig G, Quate CF, Gerber C. Atomic force microscope. Physical review letters. 1986 Mar 3;56(9):930.

26. Grassini P, Specht JE, Tollenaar M, Ciampitti I, Cassman KG. High-yield maize–soybean cropping systems in the US Corn Belt. InCrop physiology 2015 Jan 1 (pp. 17-41). Academic Press.

27. Ash M, Dohlman E. Oil crops outlook. Department of Agriculture Economic Research Service. 2013 Aug 14.

28. Liu J, Huang F, Wang X, Zhang M, Zheng R, Wang J, Yu D. Genome-wide analysis of terpene synthases in soybean: functional characterization of GmTPS3. Gene. 2014 Jul 1;544(1):83-92.

29. Chen S, Liu T, Zheng Z, Ishaq M, Liang G, Fan P, Chen T, Tang J. Recent progress and perspectives on Sb2Se3-based photocathodes for solar hydrogen production via photoelectrochemical water splitting. Journal of Energy Chemistry. 2022 Apr 1;67:508-23.

30. Shang J, Zhao LP, Yang XM, Qi XL, Yu JF, Du JB, Li K, He CS, Wang WM, Yang WY. Soybean balanced the growth and defense in response to SMV infection under different light intensities. Frontiers in Plant Science. 2023 Apr 19;14:1150870.

31. Weston-Green K, Clunas H, Jimenez Naranjo C. A review of the potential use of pinene and linalool as terpene-based medicines for brain health: discovering novel therapeutics in the flavours and fragrances of cannabis. Frontiers in Psychiatry. 2021 Aug 26;12:583211.

32. Chen X, Yauk YK, Nieuwenhuizen NJ, Matich AJ, Wang MY, Perez RL, Atkinson RG, Beuning LL. Characterisation of an (S)-linalool synthase from kiwifruit (Actinidia arguta)

that catalyses the first committed step in the production of floral lilac compounds. Functional Plant Biology. 2010 Feb 25;37(3):232-43.

33. Yang T, Stoopen G, Thoen M, Wiegers G, Jongsma MA. Chrysanthemum expressing a linalool synthase gene 'smells good', but 'tastes bad'to western flower thrips. Plant Biotechnology Journal. 2013 Sep;11(7):875-82.

34. Geron C, Guenther A, Greenberg J, Loescher HW, Clark D, Baker B. Biogenic volatile organic compound emissions from a lowland tropical wet forest in Costa Rica. Atmospheric Environment. 2002 Aug 1;36(23):3793-802.

35. Peñuelas J, Llusià J. Linking photorespiration, monoterpenes and thermotolerance in Quercus. New Phytologist. 2002 Aug;155(2):227-37.

36. Guenther A, Geron C, Pierce T, Lamb B, Harley P, Fall R. Natural emissions of non-methane volatile organic compounds, carbon monoxide, and oxides of nitrogen from North America. Atmospheric Environment. 2000 Jan 1;34(12-14):2205-30.

37. Abraham E, Matthay MA, Dinarello CA, Vincent JL, Cohen J, Opal SM, Glauser M, Parsons P, Fisher Jr CJ, Repine JE. Consensus conference definitions for sepsis, septic shock, acute lung injury, and acute respiratory distress syndrome: time for a reevaluation. Critical care medicine. 2000 Jan 1;28(1):232-5.

38. Singh HP, Batish DR, Kaur S, Arora K, Kohli RK. α-Pinene inhibits growth and induces oxidative stress in roots. Annals of Botany. 2006 Oct 7;98(6):1261-9.

39. Lin-Yao Y, Si-Yuan C, Xiao W, Jun Z, Cheng-Hong W. Digital twins and parallel systems: state of the art, comparisons and prospect. Acta Automatica Sinica. 2019;45(11):2001-31.

40. Mălinaş A, Vidican R, Rotar I, Mălinaş C, Moldovan CM, Proorocu M. Current status and future prospective for nitrogen use efficiency in wheat (Triticum aestivum L.). Plants. 2022 Jan;11(2):217.

41. Moura-Sobczak J, Souza U, Mazzafera P. Drought stress and changes in the lignin content and composition in Eucalyptus. InBMC proceedings 2011 Sep 13 (Vol. 5, No. Suppl 7, p. P103). London: BioMed Central.

42. Zheng P, Aoki D, Yoshida M, Matsushita Y, Imai T, Fukushima K. Lignification of ray parenchyma cells in the xylem of Pinus densiflora. Part I: Microscopic investigation by POM, UV microscopy, and TOF-SIMS. Holzforschung. 2014 Dec 1;68(8):897-905.

43. Fabre F, Planchon C. Nitrogen nutrition, yield and protein content in soybean. Plant Science. 2000 Mar 7;152(1):51-8.

44. Xu X, Du X, Wang F, Sha J, Chen Q, Tian G, Zhu Z, Ge S, Jiang Y. Effects of potassium levels on plant growth, accumulation and distribution of carbon, and nitrate metabolism in apple dwarf rootstock seedlings. Frontiers in Plant Science. 2020 Jun 23;11:904.

45. Roy M, Prasad A. Raman spectroscopy for nutritional stress detection in plant vascular tissue. Materialia. 2022 Aug 1;24:101474.

46. Khambhati VH, Abbas HK, Sulyok M, Tomaso-Peterson M, Chen J, Shier WT. Mellein: Production in culture by Macrophomina phaseolina isolates from soybean plants exhibiting symptoms of charcoal rot and its role in pathology. Frontiers in Plant Science. 2023 Feb 8;14:1105590.

47. Barbanti L, Grandi S, Vecchi A, Venturi G. Sweet and fibre sorghum (Sorghum bicolor (L.) Moench), energy crops in the frame of environmental protection from excessive nitrogen loads. European journal of agronomy. 2006 Jul 1;25(1):30-9.

48. Bashir MT, Ali SA, Ghauri M, Adris A, Harun RA. Impact of excessive nitrogen fertilizers on the environment and associated mitigation strategies. Asian J. Microbiol. Biotechnol. Environ. Sci. 2013 Jul;15(2):213-21.

49. Kong L, Xie Y, Hu L, Si J, Wang Z. Excessive nitrogen application dampens antioxidant capacity and grain filling in wheat as revealed by metabolic and physiological analyses. Scientific Reports. 2017 Feb 24;7(1):43363.

50. Lu ZX, Yu XP, Heong KL, Cui HU. Effect of nitrogen fertilizer on herbivores and its stimulation to major insect pests in rice. Rice Science. 2007 Mar 1;14(1):56-66.

51. Wang D, Xu Z, Zhao J, Wang Y, Yu Z. Excessive nitrogen application decreases grain yield and increases nitrogen loss in a wheat–soil system. Acta Agriculturae Scandinavica, Section B-Soil & Plant Science. 2011 Nov 1;61(8):681-92.

52. Naguib M, Kurtoglu M, Presser V, Lu J, Niu J, Heon M, Hultman L, Gogotsi Y, Barsoum MW. Two-dimensional nanocrystals produced by exfoliation of Ti3AlC2. Advanced materials. 2011 Oct 4;23(37):4248-53.

53. Barsoum MW. MAX phases: properties of machinable ternary carbides and nitrides. John Wiley & Sons; 2013 Nov 13.

54. Barsoum MW. MAX phases: properties of machinable ternary carbides and nitrides. John Wiley & Sons; 2013 Nov 13.

55. Anasori B, Lukatskaya MR, Gogotsi Y. 2D metal carbides and nitrides (MXenes) for energy storage. Nature Reviews Materials. 2017 Jan 17;2(2):1-7.

56. Tao Q, Dahlqvist M, Lu J, Kota S, Meshkian R, Halim J, Palisaitis J, Hultman L, Barsoum MW, Persson PO, Rosen J. Two-dimensional Mo1. 33C MXene with divacancy ordering prepared from parent 3D laminate with in-plane chemical ordering. Nature communications. 2017 Apr 25;8(1):14949.

57. Zhou J, Zha X, Zhou X, Chen F, Gao G, Wang S, Shen C, Chen T, Zhi C, Eklund P, Du S. Synthesis and electrochemical properties of two-dimensional hafnium carbide. ACS nano. 2017 Apr 25;11(4):3841-50.

58. Dillon AD, Ghidiu MJ, Krick AL, Griggs J, May SJ, Gogotsi Y, Barsoum MW, Fafarman AT. Highly conductive optical quality solution-processed films of 2D titanium carbide. Advanced Functional Materials. 2016 Jun;26(23):4162-8.

59. Sang X, Xie Y, Lin MW, Alhabeb M, Van Aken KL, Gogotsi Y, Kent PR, Xiao K, Unocic RR. Atomic defects in monolayer titanium carbide (Ti3C2T x) MXene. ACS nano. 2016 Oct 25;10(10):9193-200.

60. Furukawa H, Cordova KE, O'Keeffe M, Yaghi OM. The chemistry and applications of metal-organic frameworks. Science. 2013 Aug 30;341(6149):1230444.

61. Ghidiu M, Lukatskaya MR, Zhao MQ, Gogotsi Y, Barsoum MW. Conductive two-dimensional titanium carbide 'clay'with high volumetric capacitance. Nature. 2014 Dec 4;516(7529):78-81.

62. Wang X, Kajiyama S, Iinuma H, Hosono E, Oro S, Moriguchi I, Okubo M, Yamada A. Pseudocapacitance of MXene nanosheets for high-power sodium-ion hybrid capacitors. Nature communications. 2015 Apr 2;6(1):6544.

63. Liang X, Garsuch A, Nazar LF. Sulfur cathodes based on conductive MXene nanosheets for high-performance lithium–sulfur batteries. Angewandte Chemie. 2015 Mar 23;127(13):3979-83.

64. Ren CE, Hatzell KB, Alhabeb M, Ling Z, Mahmoud KA, Gogotsi Y. Charge-and size-selective ion sieving through Ti3C2T x MXene membranes. The journal of physical chemistry letters. 2015 Oct 15;6(20):4026-31.

65. Seh ZW, Fredrickson KD, Anasori B, Kibsgaard J, Strickler AL, Lukatskaya MR, Gogotsi Y, Jaramillo TF, Vojvodic A. Two-dimensional molybdenum carbide (MXene) as an efficient electrocatalyst for hydrogen evolution. ACS Energy Letters. 2016 Sep 9;1(3):589-94.

66. Shahzad F, Alhabeb M, Hatter CB, Anasori B, Man Hong S, Koo CM, Gogotsi Y. Electromagnetic interference shielding with 2D transition metal carbides (MXenes). Science. 2016 Sep 9;353(6304):1137-40.

67. Halim J, Lukatskaya MR, Cook KM, Lu J, Smith CR, Näslund LÅ, May SJ, Hultman L, Gogotsi Y, Eklund P, Barsoum MW. Transparent conductive two-dimensional titanium carbide epitaxial thin films. Chemistry of Materials. 2014 Apr 8;26(7):2374-81.

68. Hantanasirisakul K, Zhao MQ, Urbankowski P, Halim J, Anasori B, Kota S, Ren CE, Barsoum MW, Gogotsi Y. Fabrication of Ti3C2Tx MXene transparent thin films with tunable optoelectronic properties. Advanced Electronic Materials. 2016 Jun;2(6):1600050.

69. Lipatov A, Alhabeb M, Lukatskaya MR, Boson A, Gogotsi Y, Sinitskii A. Effect of synthesis on quality, electronic properties and environmental stability of individual

monolayer Ti3C2 MXene flakes. Advanced Electronic Materials. 2016 Dec;2(12):1600255.

70. Shekhirev M, Shuck CE, Sarycheva A, Gogotsi Y. Characterization of MXenes at every step, from their precursors to single flakes and assembled films. Progress in Materials Science. 2021 Jul 1;120:100757.

71. Halim J, Kota S, Lukatskaya MR, Naguib M, Zhao MQ, Moon EJ, Pitock J, Nanda J, May SJ, Gogotsi Y, Barsoum MW. Synthesis and characterization of 2D molybdenum carbide (MXene). Advanced Functional Materials. 2016 May;26(18):3118-27.

72. Zhang L, Song W, Liu H, Ding H, Yan Y, Chen R. Influencing Factors on Synthesis and Properties of MXene: A Review. Processes. 2022 Sep 1;10(9):1744.

73. Hu T, Yang J, Li W, Wang X, Li CM. Quantifying the rigidity of 2D carbides (MXenes). Physical Chemistry Chemical Physics. 2020;22(4):2115-21.

74. Jiang J, Bai S, Zou J, Liu S, Hsu JP, Li N, Zhu G, Zhuang Z, Kang Q, Zhang Y. Improving stability of MXenes. Nano Research. 2022 Jul;15(7):6551-67.

75. Liu N, Li Q, Wan H, Chang L, Wang H, Fang J, Ding T, Wen Q, Zhou L, Xiao X. High-temperature stability in air of Ti3C2T x MXene-based composite with extracted bentonite. Nature Communications. 2022 Sep 22;13(1):5551.

76. Jia G, Zheng A, Wang X, Zhang L, Li L, Li C, Zhang Y, Cao L. Flexible, biocompatible and highly conductive MXene-graphene oxide film for smart actuator and humidity sensor. Sensors and Actuators B: Chemical. 2021 Nov 1;346:130507.

77. Riazi H, Taghizadeh G, Soroush M. MXene-based nanocomposite sensors. ACS omega. 2021 Apr 20;6(17):11103-12.

78. Li X, Huang Z, Zhi C. Environmental stability of MXenes as energy storage materials. Frontiers in Materials. 2019 Dec 11;6:312.

79. Ho DH, Choi YY, Jo SB, Myoung JM, Cho JH. Sensing with MXenes: progress and prospects. Advanced Materials. 2021 Nov;33(47):2005846.

80. Boncan DA, Tsang SS, Li C, Lee IH, Lam HM, Chan TF, Hui JH. Terpenes and terpenoids in plants: Interactions with environment and insects. International Journal of Molecular Sciences. 2020 Oct 6;21(19):7382.

81. Johnson M, Koirala S, Rudie A, Zhang Q, Wang D. Nanomaterial-Based Sensing Technology for the Application in Breath Analyzer as for Early Disease Detection and Prevention. Recent Trends in Biotechnology.

82. Sheppard NF, Tucker RC, Wu C. Electrical conductivity measurements using microfabricated interdigitated electrodes. Analytical Chemistry. 1993 May 1;65(9):1199-202.

83. Mazlan NS, Ramli MM, Abdullah MM, Halin DC, Isa SM, Talip LF, Danial NS, Murad SZ. Interdigitated electrodes as impedance and capacitance biosensors: A review. InAIP Conference proceedings 2017 Sep 26 (Vol. 1885, No. 1). AIP Publishing.

84. Zhang L, Zhou M, Wang A, Zhang T. Selective hydrogenation over supported metal catalysts: from nanoparticles to single atoms. Chemical reviews. 2019 Sep 24;120(2):683-733.

85. Moeller T. Chemistry: with inorganic qualitative analysis. Elsevier; 2012 Dec 2.

86. Alhabeb M, Maleski K, Anasori B, Lelyukh P, Clark L, Sin S, Gogotsi Y. Guidelines for synthesis and processing of two-dimensional titanium carbide (Ti3C2T x MXene). Chemistry of Materials. 2017 Sep 26;29(18):7633-44.

87. Il'Ina II, Simakova IL, Semikolenov VA. Kinetics of the Hydrogenation of α-Pinene to cis- and trans-Pinanes on Pd/C. Kinetics and catalysis. 2002 Sep;43:645-51.

88. Li Z, Zhou J, Dong T, Xu Y, Shang Y. Application of electrochemical methods for the detection of abiotic stress biomarkers in plants. Biosensors and Bioelectronics. 2021 Jun 15;182:113105.

89. Ku YS, Sintaha M, Cheung MY, Lam HM. Plant hormone signaling crosstalks between biotic and abiotic stress responses. International Journal of Molecular Sciences. 2018 Oct 17;19(10):3206.

90. Zhang W, Zhao F, Jiang L, Chen C, Wu L, Liu Z. Different pathogen defense strategies in Arabidopsis: more than pathogen recognition. Cells. 2018 Dec 7;7(12):252.

91. Copolovici L, Popitanu AC, Copolovici DM. Volatile organic compound emission and residual substances from plants in light of the globally increasing CO2 level. Current Opinion in Environmental Science & Health. 2021 Feb 1;19:100216.

92. Wang W, Vinocur B, Altman A. Plant responses to drought, salinity and extreme temperatures: towards genetic engineering for stress tolerance. Planta. 2003 Nov;218:1-4.

93. Farmer DK, Riches M. Measuring biosphere–atmosphere exchange of short-lived climate forcers and their precursors. Accounts of Chemical Research. 2020 Jul 20;53(8):1427-35.

94. Im H, Lee S, Naqi M, Lee C, Kim S. Flexible PI-based plant drought stress sensor for real-time monitoring system in smart farm. Electronics. 2018 Jul 16;7(7):114.

95. Li Z, Liu Y, Hossain O, Paul R, Yao S, Wu S, Ristaino JB, Zhu Y, Wei Q. Real-time monitoring of plant stresses via chemiresistive profiling of leaf volatiles by a wearable sensor. Matter. 2021 Jul 7;4(7):2553-70.

96. Yury G, Anasori B. The rise of MXenes. Acs Nano. 2019;13:8491-4.

APPENDIX. Ti_3AlC_2 MAX AND Ti_3C_2 MXENE SYNTHESIS

Chemicals:

1. TiC powder
2. Al powder
3. Ti powder

Equipment:

1. 1700°C Tube Furnace, high purity alumina crucible
2. Ball-mill, alumina jars and balls
3. Hydraulic press, press die

Procedure:

Step 1: Ball-milling

- TiC, Al, and Ti powders are weighed out into a 2:1.2:1 molar ratio. In order to get 15 grams of the product use 9.12g TiC, 3.49g Ti, and 2.39g Al
- Place powders in ball mill jar 1 with 40ml of toluene
- Weigh out Al_2O_3 in an amount equal to the total of other materials (TiC, Ti, Al) placed in jar 1. Put Al_2O_3 in jar 2 and continuously add DI water in jar 2 until the solution in jar 2 equals to the solution present in jar 1
- Run ball-mill for 2 hours (see ball-mill instructions for setting up the run time).
- Collect the milled powder via centrifuge (see centrifuge instructions for use), and separate alumina balls beforehand. Use funnel and grate to separate alumina balls
- Dry the collected powder in vacuum oven in lab ECE 235

Step 2: Sample Preparation for Sinter

- Sintering can be done as a pellet or a powder

(a) Pellet

- To make a pellet, weigh out a 3g sample of milled pre-MAX powder
- Load sample into assembled die for pressing
- Load die into hydraulic press, and press at 5 US-tons for 1 minute
- Remove sample from die and repeat until all pre-MAX are used
- Load pellets into high-purity alumina crucible for sintering

(b) Powder

- Load dried pre-MAX powder into high-purity alumina crucible
- Be sure sample is in a single uniform "mound" in the center of crucible

Step 3: Sintering

- Sinter sample at 1350 degree Celsius for 4 hours under Ar gas flow in 1700 tube-furnace

Step 4: Preparation for Etching

- After sintering, the newly formed MAX material comes out as solid
- Separate the white powder coating from the outside using coarse sandpaper as best as possible
- Break apart MAX material by gently tapping, grinding, and wedging using various tools around lab (such as a wedge, a hammer, and alumina mortar and pedestal for best effect)
- Once sample is broken into pieces under $1cm^3$ in size, the remaining sample can be ball-milled in jar 2. This process is similar to the ball-milling in Step 1 of the procedure, where jar 1 is the broken MAX with 40ml of toluene and jar 2 is filled with Al_2O_3 and DI water
- Ball-Mill for 2 hours (see ball-mill instructions for setting up the run time).

Note: It is okay if not all sample is fine enough to move through sieve, separate and save for future manual grinding using mortar and pestle.

- Collect powder via centrifuge, and dry in vacuum in oven
- Sieve the MAX powder using finest sieve in the lab
- Collect and store the MAX powder in sealed container for future use

Step 5: HCl + LiF etching at room temperature

- The collected MAX powder is measured out in a weigh paper using a weigh machine. Weigh out the desired MAX powder (in grams) in order to do the etching
- The stoichiometric ratios measured out for HCl + LiF + MAX + DI water are as follows:
    - 1 gram MAX powder: 5 mL DI water: 15 mL HCl: 1.6 grams LiF
- At first, the HCl + DI water are measured out using a graduated cylinder and transferred into a plastic wide mouth leak proof bottle (Teflon bottle). Then, the solution is stirred using a stir bar on a stir plate for atleast 5 minutes
- The desired MAX powder and LiF powder are weigh out. After that, proper PPE must be worn such as lab coat, PVC apron, safety googles, neoprene-coated latex gloves, and face shield headgear before adding the powders in the solution
- LiF powder are slowly added into the HCl + DI water solution using a funnel and stirred for 5 minutes on a stir plate
- Then, MAX powder are added slowly into the etching solution using a funnel and stirred for 24 hours at a room temperature (about 25°C-30°C)

Step 6: Washing process

- The prepared acidic mixture (HCl + LiF + MAX) are washed with DI water via centrifugation (5 mins of run time per 6000rpm) using centrifuge tube that is filled up to 50mL for multiple cycles until a pH of 4-5 has been achieved
- Once the etching solution is neutralized, then further washing is done via centrifugation (5mins/6000rpm) until a black distinctive layer of Ti_3C_2 slurry is observed above a grayish layer of nonetched Ti_3AlC_2/Ti_3C_2 mixture

Step 7: Storage of Ti_3C_2

- Ti_3C_2 can be stored in a paste or a powdered form:
    - In order to store it in a paste form, the Ti_3C_2 paste is washed with ethanol once via centrifugation (5mins/6000rpm) using a centrifuge tube.
    - In order to store it in a powdered form, the same step is done for washing using ethanol and after that it can either be left under the fume hood for at least 2-3 days to dry or in a vacuum oven for 1 day.